JOURNAL OF THERMOPHYSICS AND HEAT TRANSFER
Vol. 16, No. 3, July–September 2002

Solidified Layer Growth and Decay Characteristics During Freeze Coating of Binary Substance

C. Tangthieng* and F. B. Cheung†
Pennsylvania State University, University Park, Pennsylvania 16802
and
Y. C. Shih‡
National Taipei University of Technology, Taipei 106, Taiwan, Republic of China

The process of freeze coating of a binary substance on a continuous moving plate is studied theoretically, taking into full account the finite thickness of the plate and the flow and heat transfer in the two-phase mushy zone adjacent to the freeze coat. A mathematical model, composed of a system of equations governing the heat transfer in the plate, the freeze coat region, the two-phase mushy zone that is subdivided into the two-phase packing and the two-phase dispersed regions, and the melt region, is developed to describe the growth and decay behavior of the freeze coat on the moving plate. The governing equations, transformed into a dimensionless space to immobilize the solidus and liquidus interface locations, are solved numerically by an implicit finite difference method. Eight dimensionless parameters of the system that control the growth and decay behavior of the freeze coat are identified, and their effects on the maximum freeze-coat thickness and the corresponding axial location are determined.

Nomenclature

b = exponent power
C_p = specific heat, J/(kg · K)
d = half of plate thickness, m
F = solid fraction
F_p = packing limit fraction
k = thermal conductivity, W/(m · K)
m_1 = slope of the solidus line
m_2 = slope of the liquidus line
Pr = Prandlt number
R_1 = wall subcooling dimensionless parameter
R_2 = liquid superheating dimensionless parameter
R_3 = freeze coat-to-wall thermal conductivity ratio
R_4 = freeze coat-to-wall heat capacity ratio
Ste = Stefan number
T = temperature, K
T_p = temperature corresponding to F_p, K
T_0 = inlet plate temperature, K
T_1 = solidus temperature corresponding to C_∞, K
T_2 = liquidus temperature corresponding to C_∞, K
T_∞ = ambient liquid temperature, K
U = axial dimensionless velocity
U_0 = plate velocity, m/s
u = axial velocity, m/s
V = vertical dimensionless velocity
v = vertical velocity, m/s
x = Cartesian coordinate in axial direction, m
y = Cartesian coordinate in vertical direction, m
α = thermal diffusivity, m^2/s
ΔH = latent heat of fusion, J/kg
Δ_p = vertical dimensionless distance corresponding to the packing limit isotherm
Δ_1 = dimensionless thickness of freeze coat or vertical dimensionless distance corresponding to the solidus isotherm
$\Delta_{1,\max}$ = dimensionless maximum thickness of freeze coat
Δ_2 = vertical dimensionless distance corresponding to the liquidus isotherm
δ_p = vertical distance corresponding to the packing limit isotherm, m
δ_1 = thickness of freeze coat corresponding to the solidus isotherm, m
δ_2 = vertical distance corresponding to the liquidus isotherm, m
η = independent similarity variable or dimensionless coordinate in vertical vertical direction
θ = dimensionless temperature
κ = equilibrium partition ratio
μ = dynamic viscosity, kg/(m · s)
$[\mu]$ = intrinsic dynamic viscosity
ν = kinematic viscosity, m^2/s
ξ = dimensionless coordinate in axial direction
$\xi_{\max}$ = dimensionless coordinate corresponding to the maximum freeze-coat thickness
ρ = density, kg/m^3
ω = stretching factor

Subscripts

ℓ = liquid region
m = two-phase mushy region
md = two-phase dispersed region
mp = two-phase packing region
s = freeze coat region
w = wall region

Received 2 July 2001; revision received 4 December 2001; accepted for publication 24 January 2002.

*Ph.D. Student, Department of Mechanical and Nuclear Engineering.
†Professor, Department of Mechanical and Nuclear Engineering.
‡Assistant Professor, Department of Air Conditioning and Refrigeration.

Introduction

A PROCESS involving the formation of a thin solidified layer on a moving object, referred to as the freeze-coating process, is considered in this study. The freeze-coating process is an important thermal manufacturing process. During a line production, the surfaces of a plate are first cleaned, and the plate is chilled below the freezing temperature of the coating material. Then, the plate is fed through a bath filled with the molten coating material, resulting in the formation of a thin solidified layer or a freeze coat. Depending on

the applications, the freeze coat can be used as a thermal insulator, electrical insulator, corrosive protector, or flame retardant.

The process of freeze coating on a semi-infinite plate has been studied by many investigators[1–4] for the case of a coating material made of a pure substance, where the solidification process occurs at a constant temperature and the interface between the freeze coat and the melt is sharp. In the study of Kuiken,[1] the wall was assumed to be isothermal. Kuiken also presented asymptotic cases for small and large Prandlt numbers. Seeniraj and Bose[2] studied the freeze-coating problem by assuming the wall temperature to be constant and the melt at the saturated temperature. Cheung[3,4] extended the work of Seeniraj and Bose[2] by accounting for the effects of superheated melt and nonisothermal wall.

The freeze-coating process with different flow arrangements has also been studied extensively. Rezaian and Poulikakos[5] investigated the effect of melt flow in a direction parallel to an isothermal moving plate. Stevens and Poulikakos[6] extended the work of Rezaian and Poulikakos[5] by using alloy melt as a coating material. In their work, Stevens and Poulikakos assumed that heat conduction is dominant in the mushy region. In the work of Zhang et al.,[7] the plate was pulled vertically from the alloy bath. The effect of buoyancy was included in the model. Zhang and Moallemi[8] extended the work of Zhang et al.[7] by taking the thermocapillary effect into account.

The growth and decay behavior of a freeze coat was investigated by Cheung and Cha.[9] In their work, the finite difference method was employed to obtain the maximum thickness of the freeze coat on a moving cylinder. An experimental verification of the theoretical analysis was conducted by Cheung et al.[10] using a copper wire to simulate a moving cylinder and water to simulate a molten substance. Mahmoud[11,12] analyzed the unsteady freeze-coating process of a polymeric substance using the finite element method. The growth and decay behavior of a freeze coat as a function of time was examined.

Most recently, the process of freeze coating of a binary substance on a chilled moving plate was studied by Tangthieng et al.,[13] who took into full account the behavior of the two-phase mushy zone in the system. In their study, however, the plate was assumed semi-infinite in thickness. There was an infinite heat capacity of the plate available so that the freeze coat continued to grow in the downstream direction without decay. Under this limiting condition, Tangthieng et al.[13] found the system to admit a similarity solution. The governing partial differential equations were transformed into a system of ordinary differential equations, which was then solved numerically to determine the rate of growth of the freeze coat.

In the present study, the freeze-coating process of a binary alloy on a moving plate with finite thickness is investigated, by including consideration the finite heat capacity of the wall and the flow and heat transfer in the two-phase mushy zone. The governing equations for five separate regions are formulated and transformed into a dimensionless form. The finite difference method is then applied to solve the transformed equations and to determine the growth and decay behavior of the freeze coat. The effects of various controlling parameters on the variations of the maximum freeze-coat thickness and the corresponding location are identified.

Problem Formulation

A schematic of the freeze-coating system under consideration is shown in Fig. 1. A finite plate with a uniform thickness of $2d$ initially at a uniform temperature T_0 is continuously fed through a bath filled with a binary alloy melt, which is kept at a constant temperature T_∞. The inlet plate temperature T_0 is lower than the solidus temperature T_1 of the binary alloy, whereas the bath temperature T_∞ is higher than the liquidus temperature T_2 of the binary alloy. As the chilled plate travels through the bath, a freeze coat begins to form on the surface of the plate and continuously grows along the immersed distance. Because of a finite heat capacity of the plate, at a certain downstream location x_{max}, the freeze coat would reach its maximum thickness $\delta_{1,max}$ and begin to remelt thereafter, as shown in Fig. 1. The locations δ_1 and δ_2 represent the isothermal contours of the solidus and liquidus temperatures, respectively.

The region between δ_1 and δ_2 is the two-phase mushy zone (Fig. 2) where the solid and liquid phases can coexist over a range of temperatures, that is, from T_1 to T_2. Based on the value of the mixture viscosity, the mushy zone can be divided into two subregions: the two-phase packing region and two-phase dispersed region. When the solid fraction F in the mushy zone is larger than the packing limit fraction F_p, the dendrites start locking and packing to one another, resulting in the formation of a rigid structure trapping liquid inside.[14,15] The viscosity of this solid structure asymptotically approaches infinity. This region of a solidlike structure is referred to as the two-phase packing region. On the other hand, when F is lower than F_p, the viscosity of the mixture reduces drastically, and the mixture is able to move relative to the plate. Under forced convection conditions, the fluid flow can cause the dendritic structure to break off.[16] The broken dendrites flowing with an interdendrite liquid may behave like a flow with dispersed suspension. This region is referred to as the two-phase dispersed region.

To formulate the governing equations for the freeze-coating process, several simplifying assumptions are made: 1) The alloy melt is assumed to be a Newtonian fluid. 2) The freeze-coating process is steady, and the flow is laminar. Note that the occurrence of transition-to-turbulent flow may cause a sudden reduction of the freeze-coat thickness, which is not desirable during the manufacturing process.[17] 3) A boundary-layer forced convection flow is assumed in the two-phase dispersed region and the melt region. This assumption is considered valid because the thickness of the plate is much smaller than the immersion distance, that is, the length of the plate in the bath. 4) Physical properties of each phase may be

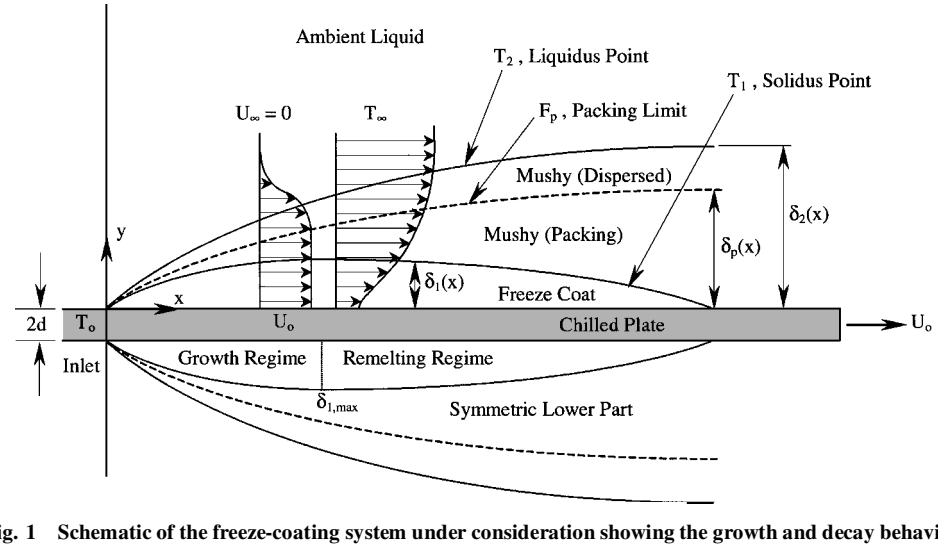

Fig. 1 Schematic of the freeze-coating system under consideration showing the growth and decay behavior.

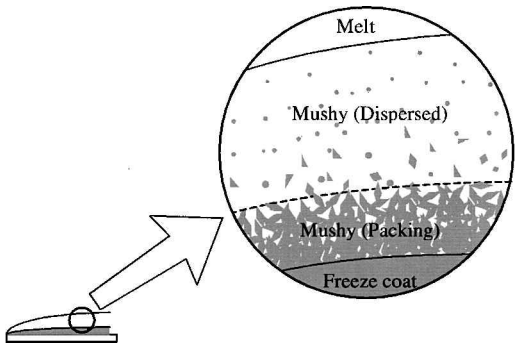

Fig. 2 Configuration of the two-phase mushy zone consisting of the packing and the dispersed regions.

treated constant. The properties for the mushy zone are taken to be the weighted average of the physical properties for each individual phase. However, a separate supplemental equation for the viscosity of the mushy zone is required as discussed later. 5) Local thermodynamic equilibrium exists such that the value of the solid fraction can be directly evaluated from the phase diagram. 6) In the two-phase dispersed region, the velocity of the broken dendrites and the interdendrite liquid are equal, resulting in the absence of the dispersion flux terms in the momentum and energy equation.[18] 7) During the solidification process, the constituent concentration is constant. Because of the effect of the main flow, the rejected solute concentration at the liquidus temperature may be washed away and replaced by the ambient concentration.[16,19]

With the aforementioned assumptions, the governing equations with associated boundary conditions for each individual region can be written as follows.

Wall region ($x \geq 0$ and $-d \leq y \leq 0$):

$$\rho_w C_{P_w} U_0 \frac{\partial T_w}{\partial x} = k_w \frac{\partial^2 T_w}{\partial y^2} \tag{1}$$

$$x = 0 : T_w = T_0 \tag{2a}$$

$$y = 0 : T_w = T_s, \qquad k_w \frac{\partial T_w}{\partial y} = k_s \frac{\partial T_s}{\partial y} \tag{2b}$$

$$y = -d : k_w \frac{\partial T_w}{\partial y} = 0 \tag{2c}$$

Freeze-coat region ($x \geq 0$ and $0 \leq y \leq \delta_1$):

$$\rho_s C_{P_s} U_0 \frac{\partial T_s}{\partial x} = k_s \frac{\partial^2 T_s}{\partial y^2} \tag{3}$$

$$x = 0 : \delta_1 = 0 \tag{4a}$$

$$y = 0 : T_s = T_w, \qquad k_s \frac{\partial T_s}{\partial y} = k_w \frac{\partial T_w}{\partial y} \tag{4b}$$

$$y = \delta_1 : T_s = T_1, \qquad \frac{\partial T_s}{\partial y} = \frac{\partial T_{mp}}{\partial y} \tag{4c}$$

Two-phase packing region ($x \geq 0$ and $\delta_1 \leq y \leq \delta_p$):

$$U_0 \frac{\partial T_{mp}}{\partial x} = \alpha_m \frac{\partial^2 T_{mp}}{\partial y^2} + \frac{\Delta H_m}{C_{P_m}} U_0 \frac{\partial F}{\partial x} \tag{5}$$

$$x = 0 : \delta_p = 0 \tag{6a}$$

$$y = \delta_1 : T_{mp} = T_1, \qquad \frac{\partial T_{mp}}{\partial y} = \frac{\partial T_s}{\partial y} \tag{6b}$$

$$y = \delta_p : T_{mp} = T_p, \qquad \frac{\partial T_{mp}}{\partial y} = \frac{\partial T_{md}}{\partial y} \tag{6c}$$

Two-phase dispersed region ($x \geq 0$ and $\delta_p \leq y \leq \delta_2$):

$$\frac{\partial u_{md}}{\partial x} + \frac{\partial v_{md}}{\partial y} = 0 \tag{7}$$

$$u_{md} \frac{\partial u_{md}}{\partial x} + v_{md} \frac{\partial u_{md}}{\partial y} = \frac{\partial}{\partial y}\left(\nu_m \frac{\partial u_{md}}{\partial y}\right) \tag{8}$$

$$u_{md} \frac{\partial T_{md}}{\partial x} + v_{md} \frac{\partial T_{md}}{\partial y} = \alpha_m \frac{\partial^2 T_{md}}{\partial y^2} + \frac{\Delta H_m}{C_{P_m}}\left(u_{md} \frac{\partial F}{\partial x} + v_{md} \frac{\partial F}{\partial y}\right) \tag{9}$$

$$x = 0 : \delta_2 = 0 \tag{10a}$$

$$y = \delta_p : u_{md} = U_0, \qquad v_{md} = 0, \qquad T_{md} = T_p$$

$$\frac{\partial T_{md}}{\partial y} = \frac{\partial T_{mp}}{\partial y} \tag{10b}$$

$$y = \delta_2 : u_{md} = u_\ell, \qquad \frac{\partial u_{md}}{\partial y} = \frac{\partial u_\ell}{\partial y}, \qquad v_{md} = v_\ell$$

$$T_{md} = T_2, \qquad \frac{\partial T_{md}}{\partial y} = \frac{\partial T_\ell}{\partial y} \tag{10c}$$

Melt region ($x \geq 0$ and $y \geq \delta_2$):

$$\frac{\partial u_\ell}{\partial x} + \frac{\partial v_\ell}{\partial y} = 0 \tag{11}$$

$$u_\ell \frac{\partial u_\ell}{\partial x} + v_\ell \frac{\partial u_\ell}{\partial y} = \nu_\ell \frac{\partial^2 u_\ell}{\partial y^2} \tag{12}$$

$$u_\ell \frac{\partial T_\ell}{\partial x} + v_\ell \frac{\partial T_\ell}{\partial y} = \alpha_\ell \frac{\partial^2 T_\ell}{\partial y^2} \tag{13}$$

$$x = 0 : u_\ell = 0, \qquad T_\ell = T_\infty \tag{14a}$$

$$y = \delta_2 : u_\ell = u_{md}, \qquad v_\ell = v_{md}, \qquad \frac{\partial u_\ell}{\partial y} = \frac{\partial u_{md}}{\partial y}$$

$$T_\ell = T_2, \qquad \frac{\partial T_\ell}{\partial y} = \frac{\partial T_{md}}{\partial y} \tag{14b}$$

$$y \to \infty : u_\ell = 0, \qquad T_\ell = T_\infty \tag{14c}$$

The latent heat term involving ΔH_m is included in the last term of Eqs. (5) and (9). Because of the absence of a vertical component of the velocity in the two-phase packing region, the latent heat effect is restricted to that in the axial direction only. On the contrary, the latent heat effect is two dimensional in the two-phase dispersed region. Note that the governing system for the two-phase packing region can be obtained from that for the two-phase dispersed region by setting $u_{md} = U_0$ and $v_{md} = 0$, where Eqs. (7) and (8) are automatically satisfied on both sides and Eq. (9) becomes identical to Eq. (5). The boundary conditions at the interface between each two adjacent regions result in a strong coupling of the equations governing the five distinct regions. The interface between the two-phase packing and two-phase dispersed region is located at δ_p, corresponding to the packing limit fraction F_p and the packing limit isotherm T_p.

To close the system of equations, an expression for the solid fraction in terms of the local temperature is needed, which can be obtained from the phase diagram. When the solidus and liquidus points are approximated by straight lines,[20] a typical phase diagram of a binary alloy can be represented in Fig. 3. The shaded area in Fig. 3 represents the isomorphous (or complete soluble) region, whereas the remaining area is the region with the formation of the eutectic structure during the solidification process. In the present study, the freeze-coating process is restricted to the isomorphous

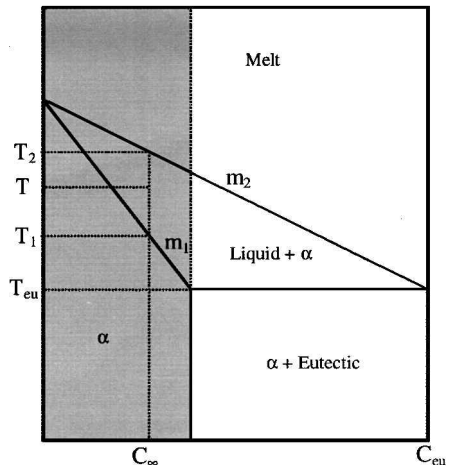

Fig. 3 Phase diagram for a binary substance considered in the present study.

region in which the solid fraction can be derived by applying the lever rule:

$$F = \frac{T_2 - T_m}{(T_2 - T_m) + \kappa(T_m - T_1)} \tag{15}$$

where T_m is the local temperature of the two-phase mushy zone (including both the two-phase packing and two-phase dispersed regions) and κ is the equilibrium partition ratio defined as the ratio of the slope of the liquidus line to that of the solidus line. Note that the solid fraction depends not only on the local temperature T_m but also on the value of κ. For the special case of $\kappa = 1$, the solid fraction is simply given by $F = (T_2 - T_m)/(T_2 - T_1)$.

The properties of the two-phase packing and dispersed regions (represented by subscript m), including the density, specific heat, and thermal conductivity, are calculated by taking an average over the properties of each individual phase weighted by the solid fraction, that is,

$$\rho_m = [(1 - F)/\rho_\ell + F/\rho_s]^{-1} \tag{16}$$

$$C_{P_m} = (1 - F)C_{P_\ell} + FC_{P_s} \tag{17}$$

$$k_m = (\rho_m/\rho_\ell)(1 - F)k_\ell + (\rho_m/\rho_s)Fk_s \tag{18}$$

The variations of the thermal properties of the two-phase mixture in the mushy zone are of secondary importance as compared to the variation in the viscosity. To minimize the number of parameters, the density, specific heat, and thermal conductivity of the freeze coat and the melt are treated to be the same. As a result, the thermal properties of the two-phase mushy zone are no longer a function of the solid fraction and have the same values as those of the freeze coat and the melt.

On the other hand, the viscosity of the two-phase dispersed region is modeled as the viscosity of dispersions (see assumption 6). Einstein[21] was the first to derive analytically an expression for the viscosity of dispersed spherical particles as a function of solid fraction and intrinsic viscosity. He showed that the value of the intrinsic viscosity asymptotically approached 2.5 for a dilute solution. To include the effect of high concentration and maximum packing limit, Krieger and Daugherty[22] theoretically derived an expression for the viscosity of dispersions, which can be written as follows:

$$\mu_m = \mu_\ell(1 - F/F_p)^{-[\mu]F_p} \tag{19}$$

In terms of the kinematic viscosity, the preceding expression becomes

$$\nu_m = \nu_\ell(1 - F/F_p)^{-[\mu]F_p} \tag{20}$$

where F_p is the maximum packing limit. Equation (19), verified experimentally by Krieger,[14] is known as the Krieger–Daugherty equation. The value of F_p may vary from 0.5 to 0.75 depending on the structure of the two-phase mixture.[23] Equations (15) and (20) provide a closure for the system of equations for the two-phase dispersed region.

Solution Methodology

Coordinate Transformation

The system of equations, that is, Eqs. (1–15) and (20), is solved numerically by using a fully implicit finite difference method with the secant iterative technique. To facilitate the computation procedure, coordinate transformation from the physical domain to a computation domain is invoked. The purpose of the transformation is to fix the interface between any two adjacent regions.[24] The following new coordinate axes and new independent variables are introduced.

Wall region:

$$\xi = x\alpha_s \big/ U_0 d^2, \qquad \eta_w = y/d, \qquad \theta_w = (T_w - T_0)/(T_1 - T_0) \tag{21}$$

where $\xi \geq 0$, $-1 \leq \eta_w \leq 0$, and $0 \leq \theta_w \leq \theta_w(0) = \theta_s(0)$.

Freeze-coat region:

$$\xi = x\alpha_s \big/ U_0 d^2, \qquad \Delta_1 = \delta_1/d, \qquad \eta_s = y/\delta_1 = y/\Delta_1 d$$
$$\theta_s = (T_s - T_0)/(T_1 - T_0) \tag{22}$$

where $\xi \geq 0$, $0 \leq \eta_s \leq 1$, and $\theta_w(0) = \theta_s(0) \leq \theta_s \leq 1$.

Two-phase mushy region:

$$\xi = \frac{x\alpha_s}{U_0 d^2}, \qquad \Delta_2 = \frac{\delta_2}{d}$$

$$\eta_m = 1 + \frac{y - \delta_1}{\delta_2 - \delta_1} = 1 + \frac{y - \Delta_1 d}{(\Delta_2 - \Delta_1)d}, \qquad U_m = \frac{u_m}{U_0}$$

$$V_m = \frac{v_m d}{\alpha_s}, \qquad \theta_m = 1 + \frac{T_m - T_1}{T_2 - T_1} \tag{23}$$

where $\xi \geq 0$, $1 \leq \eta_m \leq 2$, $U_\ell(2) = U_m(2) \leq U_m \leq 1$, $0 \leq V_m \leq V_m(2) = V_\ell(2)$, and $1 \leq \theta_m \leq 2$.

Melt region:

$$\xi = x\alpha_s \big/ U_0 d^2$$

$$\eta_\ell = 3 - \exp[\omega(1 - y/\delta_2)] = 3 - \exp[\omega(1 - y/\Delta_2 d)]$$

$$U_\ell = u_\ell/U_0, \qquad V_\ell = v_\ell d/\alpha_s, \qquad \theta_\ell = 2 + (T_\ell - T_2)/(T_\infty - T_2) \tag{24}$$

where $\xi \geq 0$, $2 \leq \eta_\ell \leq 3$, $0 \leq U_\ell \leq U_\ell(2) = U_m(2)$, $V_\ell \geq V_\ell(2) = V_m(2)$, and $2 \leq \theta_1 \leq 3$.

Because the governing equations for the two-phase packing region can be obtained from those for the two-phase dispersed region, in the computational domain these two domains are combined together by using the same independent and dependent variables. Note that in Eq. (24) the exponential relation is applied to transform the semi-infinite domain in the melt region into a finite one.[25] The quantity ω is a stretching factor, which represents how much the η coordinate has been stretched in the melt region. A larger value of ω will provide a clustered grid near the interface, whereas a smaller one will further stretch the grid. The value of ω used in the present computer program is between 0.1 and 0.5.

When Eqs. (21–24) are substituted into Eqs. (1–14), the governing equations in the computational domain can be written as follows.

Wall region ($\xi \geq 0$, $-1 \leq \eta_w \leq 0$):

$$\frac{\partial^2 \theta_w}{\partial \eta_w^2} - \frac{R_3}{R_4}\frac{\partial \theta_w}{\partial \xi} = 0 \tag{25}$$

$$\xi = 0 : \theta_w = 0 \tag{26a}$$

$$\eta_w = 0 : \theta_w = \theta_s, \qquad \Delta_1 \frac{\partial \theta_w}{\partial \eta_w} = R_3 \frac{\partial \theta_s}{\partial \eta_s} \tag{26b}$$

$$\eta_w = -1 : \frac{\partial \theta_w}{\partial \eta_w} = 0 \tag{26c}$$

Freeze-coat region ($\xi \geq 0$, $0 \leq \eta_s \leq 1$):

$$\frac{\partial^2 \theta_s}{\partial \eta_s^2} + \eta_s \Delta_1 \frac{\mathrm{d}\Delta_1}{\mathrm{d}\xi} \frac{\partial \theta_s}{\partial \eta_s} - \Delta_1^2 \frac{\partial \theta_s}{\partial \xi} = 0 \tag{27}$$

$$\xi = 0 : \Delta_1 = 0 \tag{28a}$$

$$\eta_s = 0 : \theta_s = \theta_w, \qquad R_3 \frac{\partial \theta_s}{\partial \eta_s} = \Delta_1 \frac{\partial \theta_w}{\partial \eta_w} \tag{28b}$$

$$\eta_s = 1 : \theta_s = 1, \qquad (\Delta_2 - \Delta_1) \frac{\partial \theta_s}{\partial \eta_s} = \frac{\Delta_1}{R_1} \frac{\partial \theta_m}{\partial \eta_m} \tag{28c}$$

Two-phase mushy region ($\xi \geq 0$, $1 \leq \eta_m \leq 2$):

$$(\Delta_2 - \Delta_1) \frac{\partial U_m}{\partial \xi} - \left[\frac{\mathrm{d}\Delta_1}{\mathrm{d}\xi} + (\eta_m - 1) \left(\frac{\mathrm{d}\Delta_2}{\mathrm{d}\xi} - \frac{\mathrm{d}\Delta_1}{\mathrm{d}\xi} \right) \right] \frac{\partial U_m}{\partial \eta_m} + \frac{\partial V_m}{\partial \eta_m} = 0 \tag{29}$$

$$\begin{aligned} &\frac{1}{Pr} (\Delta_2 - \Delta_1)^2 \left(1 - \frac{F}{F_p} \right)^b U_m \frac{\partial U_m}{\partial \xi} - \frac{1}{Pr} (\Delta_2 - \Delta_1) \left(1 - \frac{F}{F_p} \right)^b \\ &\quad \times \left[\frac{\mathrm{d}\Delta_1}{\mathrm{d}\xi} + (\eta_m - 1) \left(\frac{\mathrm{d}\Delta_2}{\mathrm{d}\xi} - \frac{\mathrm{d}\Delta_1}{\mathrm{d}\xi} \right) \right] U_m \frac{\partial U_m}{\partial \eta_m} \\ &\quad + \frac{1}{Pr} (\Delta_2 - \Delta_1) \left(1 - \frac{F}{F_p} \right)^b V_m \frac{\partial U_m}{\partial \eta_m} = \frac{\partial^2 U_m}{\partial \eta_m^2} \\ &\quad - \frac{b\kappa}{F_p} \frac{(1 - F/F_p)^{-1}}{[(2 - \theta_m) + \kappa(\theta_m - 1)]^2} \frac{\partial \theta_m}{\partial \eta_m} \frac{\partial U_m}{\partial \eta_m} \end{aligned} \tag{30}$$

$$\begin{aligned} &\left[1 + \frac{\kappa \cdot Ste^{-1}}{[(2 - \theta_m) + \kappa(\theta_m - 1)]^2} \right] (\Delta_2 - \Delta_1)^2 U_m \frac{\partial \theta_m}{\partial \xi} \\ &\quad - \left[1 + \frac{\kappa \cdot Ste^{-1}}{[(2 - \theta_m) + \kappa(\theta_m - 1)]^2} \right] (\Delta_2 - \Delta_1) \\ &\quad \times \left[\frac{\mathrm{d}\Delta_1}{\mathrm{d}\xi} + (\eta_m - 1) \left(\frac{\mathrm{d}\Delta_2}{\mathrm{d}\xi} - \frac{\mathrm{d}\Delta_1}{\mathrm{d}\xi} \right) \right] U_m \frac{\partial \theta_m}{\partial \eta_m} \\ &\quad + \left[1 + \frac{\kappa \cdot Ste^{-1}}{[(2 - \theta_m) + \kappa(\theta_m - 1)]^2} \right] (\Delta_2 - \Delta_1) V_m \frac{\partial \theta_m}{\partial \eta_m} = \frac{\partial^2 \theta_m}{\partial \eta_m^2} \end{aligned} \tag{31}$$

$$\xi = 0 : \Delta_2 = 0 \tag{32a}$$

$$\eta_m = 1 : U_m = 1, \qquad V_m = 0, \qquad \theta_m = 1$$

$$\Delta_1 \frac{\partial \theta_m}{\partial \eta_m} = R_1 (\Delta_2 - \Delta_1) \frac{\partial \theta_s}{\partial \eta_s} \tag{32b}$$

$$\eta_m = 2 : U_m = U_\ell, \qquad V_m = V_\ell$$

$$\Delta_2 \frac{\partial U_m}{\partial \eta_m} = (\Delta_2 - \Delta_1) \omega \frac{\partial U_\ell}{\partial \eta_\ell}, \qquad \theta_m = 2$$

$$\Delta_2 \frac{\partial \theta_m}{\partial \eta_m} = R_2 (\Delta_2 - \Delta_1) \omega \frac{\partial \theta_\ell}{\partial \eta_\ell} \tag{32c}$$

Melt region ($\xi \geq 0, 2 \leq \eta_\ell \leq 3$):

$$\Delta_2 \frac{\partial U_\ell}{\partial \xi} - (3 - \eta_\ell)[\omega - \ell n(3 - \eta_\ell)] \frac{\mathrm{d}\Delta_2}{\mathrm{d}\xi} \frac{\partial U_\ell}{\partial \eta_\ell} + (3 - \eta_\ell) \omega \frac{\partial V_\ell}{\partial \eta_\ell} = 0 \tag{33}$$

$$\begin{aligned} &\frac{1}{Pr} \Delta_2^2 U_\ell \frac{\partial U_\ell}{\partial \xi} - \frac{1}{Pr} (3 - \eta_\ell)(\omega - \ell n(3 - \eta_\ell)) \Delta_2 \frac{\mathrm{d}\Delta_2}{\mathrm{d}\xi} U_\ell \frac{\partial U_\ell}{\partial \eta_\ell} \\ &\quad + \frac{1}{Pr} (3 - \eta_\ell) \omega \Delta_2 V_\ell \frac{\partial U_\ell}{\partial \eta_\ell} = -(3 - \eta_\ell) \omega^2 \frac{\partial U_\ell}{\partial \eta_\ell} \\ &\quad + (3 - \eta_\ell)^2 \omega^2 \frac{\partial^2 U_\ell}{\partial \eta_\ell^2} \end{aligned} \tag{34}$$

$$\begin{aligned} &\Delta_2^2 U_\ell \frac{\partial \theta_\ell}{\partial \xi} - (3 - \eta_\ell)[\omega - \ell n(3 - \eta_\ell)] \Delta_2 \frac{\mathrm{d}\Delta_2}{\mathrm{d}\xi} U_\ell \frac{\partial \theta_\ell}{\partial \eta_\ell} \\ &\quad + (3 - \eta_\ell) \omega \Delta_2 V_\ell \frac{\partial \theta_\ell}{\partial \eta_\ell} = -(3 - \eta_\ell) \omega^2 \frac{\partial \theta_\ell}{\partial \eta_\ell} \\ &\quad + (3 - \eta_\ell)^2 \omega^2 \frac{\partial^2 \theta_\ell}{\partial \eta_\ell^2} \end{aligned} \tag{35}$$

$$\eta_\ell = 2 : U_\ell = U_m, \qquad V_\ell = V_m, \qquad (\Delta_2 - \Delta_1) \omega \frac{\partial U_\ell}{\partial \eta_\ell} = \Delta_2 \frac{\partial U_m}{\partial \eta_m}$$

$$\theta_\ell = 2, \qquad R_2 (\Delta_2 - \Delta_1) \omega \frac{\partial \theta_\ell}{\partial \eta_\ell} = \Delta_2 \frac{\partial \theta_m}{\partial \eta_m} \tag{36a}$$

$$\eta_\ell = 3 : U_\ell = 0, \qquad \theta_\ell = 3 \tag{36b}$$

The expression for the solid fraction [Eq. (15)] becomes

$$F = \frac{2 - \theta_m}{(2 - \theta_m) + \kappa(\theta_m - 1)} \tag{37}$$

Eight dimensionless parameters have been identified as the controlling parameters of the freeze-coating process. These parameters are the wall subcooling parameter R_1, the melt superheating parameter R_2, the freeze coat-to-wall thermal conductivity ratio R_3, the freeze coat-to-wall heat capacity ratio R_4, the Prandtl number Pr, the Stefan number Ste, the equilibrium partition ratio κ, and the exponent b in Eq. (20), that is,

$$R_1 = \frac{T_1 - T_0}{T_2 - T_1}, \qquad R_2 = \frac{T_\infty - T_2}{T_2 - T_1}, \qquad R_3 = \frac{k_s}{k_w}$$

$$R_4 = \frac{\rho_s C_{P_s}}{\rho_w C_{P_w}}, \qquad Pr = \frac{\nu_\ell}{\alpha_\ell}, \qquad Ste = \frac{C_{p_m}(T_2 - T_1)}{\Delta H_m}$$

$$\kappa = \frac{m_2}{m_1}, \qquad b = [\mu] F_p = 2.5 F_p \tag{38}$$

Note that, in recent years, many investigators[7,8,18] have proposed and solved full field models for binary solidification using finite volume or finite element techniques. Transitions from one region to another are handled implicitly by property variations as functions of temperature and volume fraction. From a computational point of view, this single-domain approach is very attractive because it greatly simplifies the numerical solution procedure. Nevertheless, the present computational method is chosen because it facilitates the determination of the effects of the controlling parameters on the growth and decay characteristics of a freeze coat in an explicit manner.

Finite Difference Analysis

To formulate the finite difference equations for the governing system, a fully implicit scheme is employed to eliminate the stability constraint. These equations can be written in a general form as

$$\frac{\partial^2 \varphi_r}{\partial \eta_r^2} + K_r \frac{\partial \varphi_r}{\partial \eta_r} - L_r \frac{\partial \varphi_r}{\partial \xi} = 0 \tag{39}$$

where subscript r refers to a given region, φ represents U or θ for that region, and K_r and L_r are linearized coefficients in front of the derivative terms. The central difference and forward difference formulas are applied to the derivative term in the η and ξ directions, respectively:

$$\frac{\partial^2\varphi_r}{\partial\eta_r^2} \approx \frac{\varphi_{r,\xi+1}^{\eta_r+1} - 2\varphi_{r,\xi+1}^{\eta_r} + \varphi_{r,\xi+1}^{\eta_r-1}}{\Delta\eta_r^2}, \qquad \frac{\partial\varphi_r}{\partial\eta_r} \approx \frac{\varphi_{r,\xi+1}^{\eta_r+1} - \varphi_{r,\xi+1}^{\eta_r-1}}{2\Delta\eta_r}$$

$$\frac{\partial\varphi_r}{\partial\xi} \approx \frac{\varphi_{r,\xi+1}^{\eta_r} - \varphi_{r,\xi}^{\eta_r}}{\Delta\xi} \tag{40}$$

Substituting these finite difference formulas into Eq. (39) and rearranging unknowns to the left-hand side yields

$$\left(1 + \frac{\Delta\eta_r}{2}K_r\right)\varphi_{r,\xi+1}^{\eta_r+1} - \left(2 + \frac{\Delta\eta_r^2}{\Delta\xi}L_r\right)\varphi_{r,\xi+1}^{\eta_r} + \left(1 - \frac{\Delta\eta_r}{2}K_r\right)\varphi_{r,\xi+1}^{\eta_r-1} = -\frac{\Delta\eta_r^2}{\Delta\xi}L_r\varphi_{r,\xi}^{\eta_r} \tag{41}$$

For a node located at the interface, its adjacent nodes lie on two different regions, which are governed by the following differential equations:

$$\frac{\partial^2\varphi}{\partial\eta_{r1}^2} + K_{r1}\frac{\partial\varphi}{\partial\eta_{r1}} - L_{r1}\frac{\partial\varphi}{\partial\xi} = 0 \tag{42}$$

$$\frac{\partial^2\varphi}{\partial\eta_{r2}^2} + K_{r2}\frac{\partial\varphi}{\partial\eta_{r2}} - L_{r2}\frac{\partial\varphi}{\partial\xi} = 0 \tag{43}$$

where subscripts $r1$ and $r2$ represent the two adjacent regions. The additional flux condition at the interface is generally written as

$$M_{r1}\frac{\partial\varphi}{\partial\eta_{r1}} = M_{r2}\frac{\partial\varphi}{\partial\eta_{r2}} \tag{44}$$

where M is the coefficient appearing in the flux condition. When the Taylor's series expansion with the method of weight residual is applied and combined with the flux condition at the interface, the following finite difference equation for a node located at a given interface is obtained:

$$\begin{aligned}
&\frac{2}{(2+K_{r1}\Delta\eta_{r1})}\varphi_{\xi+1}^{\eta-1} - \left[\left(2 + \frac{L_{r1}\Delta\eta_{r1}^2}{\Delta\xi}\right)\frac{1}{(2+K_{r1}\Delta\eta_{r1})}\right.\\
&\quad\left. + \left(\frac{2\Delta\eta_{r1}}{\Delta\eta_{r2}} + \frac{L_{r2}\Delta\eta_{r1}\Delta\eta_{r2}}{\Delta\xi}\right)\frac{M_{r2}}{(2-K_{r2}\Delta\eta_{r2})M_{r1}}\right]\varphi_{\xi+1}^{\eta}\\
&\quad + \frac{2}{(2-K_{r2}\Delta\eta_{r2})}\left(\frac{M_{r2}\Delta\eta_{r1}}{M_{r1}\Delta\eta_{r2}}\right)\varphi_{\xi+1}^{\eta+1}\\
&= \left[\left(\frac{L_{r1}\Delta\eta_{r1}^2}{\Delta\xi}\right)\frac{-1}{(2+K_{r1}\Delta\eta_{r1})}\right.\\
&\quad\left. + \left(\frac{L_{r2}\Delta\eta_{r1}\Delta\eta_{r2}}{\Delta\xi}\right)\frac{-M_{r2}}{(2-K_{r2}\Delta\eta_{r2})M_{r1}}\right]\varphi_{\xi}^{\eta}
\end{aligned} \tag{45}$$

On the other hand, an explicit scheme is adopted to obtain the finite difference equations for the continuity equations (29) and (33). The general form of the continuity equations can be written as

$$K_r\frac{\partial U_r}{\partial\xi} - L_r\frac{\partial U_r}{\partial\eta_r} + \frac{\partial V_r}{\partial\eta_r} = 0 \tag{46}$$

The finite difference formulas for the derivative terms are given by

$$\frac{\partial U_r}{\partial\xi} \approx \frac{1}{2}\left[\frac{U_{r,\xi+1}^{\eta_r} - U_{r,\xi}^{\eta_r}}{\Delta\xi} + \frac{U_{r,\xi+1}^{\eta_r+1} - U_{r,\xi}^{\eta_r+1}}{\Delta\xi}\right]$$

$$\frac{\partial U_r}{\partial\eta_r} \approx \frac{U_{r,\xi+1}^{\eta_r+1} - U_{r,\xi+1}^{\eta_r}}{\Delta\eta_r}, \qquad \frac{\partial V_r}{\partial\eta_r} \approx \frac{V_{r,\xi+1}^{\eta_r+1} - V_{r,\xi+1}^{\eta_r}}{\Delta\eta_r} \tag{47}$$

Substituting the preceding formulas into Eq. (46) and rearranging the equation gives

$$V_{r,\xi+1}^{\eta_r+1} = V_{r,\xi+1}^{\eta_r} + L_r\left(U_{r,\xi+1}^{\eta_r+1} - U_{r,\xi+1}^{\eta_r}\right) - \frac{K_r\Delta\eta_r}{2\Delta\xi}\left(U_{r,\xi+1}^{\eta_r} - U_{r,\xi}^{\eta_r} + U_{r,\xi+1}^{\eta_r+1} - U_{r,\xi}^{\eta_r+1}\right) \tag{48}$$

From assumption 3, the boundary-layer-type equations can be numerically solved by marching through a timelike coordinate. A well-posed initial condition is necessary to start the algorithm. The actual initial condition in the physical system is at $\xi = 0$, where Δ_1 and Δ_2 are zero. However, this initial condition provides some difficulty with the computational algorithm due to the singularity behavior at $\xi = 0$. An alternative approach is to find a solution at a sufficiently small value of ξ, for example, ξ_0, where δ_1 and δ_2 remain very thin relative to the half plate thickness d. It follows that for $\xi \le \xi_0$ the wall region can be treated as a semi-infinite domain. The freeze-coating system for a semi-infinite plate has been recently investigated by Tangthieng et al.,[13] who, for the limiting case of an infinite wall capacity, found the system to admit a similarity solution. The similarity solution presented by Tangthieng et al.[13] is employed in this study to obtain an alternate initial condition for the finite difference scheme.

For a given set of parameters given by Eq. (38), the primary unknown quantities U, V, θ, Δ_1, Δ_2, $d\Delta_1/d\xi$, and $d\Delta_2/d\xi$ can be computed from the finite difference equations. Once a value of ξ_0 is chosen and the initial condition is determined, the values of U, V, and θ at the next ξ location, for example, $\xi_0 + \Delta\xi$, can be calculated by solving the momentum, continuity, and energy equations, respectively. For the momentum and energy equations (25), (27), (30), (31), (34), and (35), the values of linearized coefficients in Eq. (39) can be calculated by using the values at the ξ_0 location. This method is referred to as the lagging coefficient technique, which is commonly used in solving a nonlinear problem.[26] Note that a system of linear algebraic equations formulated from Eq. (39) will lead to a tridiagonal matrix, which can be solved by employing the Thomas algorithm. An iterative method is utilized to update the values of U and θ until the solution converges. A residual of a solution vector, defined by a uniform vector norm, must be less than 10^{-7}. For the continuity equations (29) and (33), the value of V can be explicitly obtained by Eq. (48).

The values of Δ_1 and Δ_2 at the $\xi + \Delta\xi$ location is estimated in terms of the values of Δ_1, Δ_2, $d\Delta_1/d\xi$, and $d\Delta_2/d\xi$ at the previous ξ location. Thereafter, the estimated values of $d\Delta_1/d\xi$ and $d\Delta_2/d\xi$ at the $\xi + \Delta\xi$ location are determined by the following second-order finite difference formulas:

$$\left.\frac{\partial\Delta_1}{\partial\xi}\right|_{\xi+\Delta\xi} \approx \frac{3\Delta_1|_{\xi+\Delta\xi} - 4\Delta_1|_{\xi} + \Delta_1|_{\xi-\Delta\xi}}{\Delta\xi^2} \tag{49}$$

$$\left.\frac{\partial\Delta_2}{\partial\xi}\right|_{\xi+\Delta\xi} \approx \frac{3\Delta_2|_{\xi+\Delta\xi} - 4\Delta_2|_{\xi} + \Delta_2|_{\xi-\Delta\xi}}{\Delta\xi^2} \tag{50}$$

The secant iterative technique is implemented to update the values of Δ_1 and Δ_2 until the matching conditions at the solidus and liquidus temperatures, that is, $\theta_s(1) = \theta_m(1) = 1$ and $\theta_m(2) = \theta_\ell(2) = 2$, are satisfied. The convergence criteria for these two conditions are set equal to 10^{-7}. After all convergence criteria are satisfied, the program will move to the next ξ location and march forward until the value of Δ_1 reaches the maximum.

A baseline case, that is, $R_1 = 5$, $R_2 = 1$, $R_3 = 1$, $R_4 = 1$, $Pr = 0.1$, $Ste = 0.1$, $\kappa = 0.3$, and $F_p = 0.6$, has been chosen to examine the grid independency of the solutions. The effects of the step size in the ξ and η directions ($\Delta\xi$ and $\Delta\eta$, respectively), the initial location ξ_0, and the stretching factor ω were investigated to verify the numerical accuracy of the results. It was found that for $0.1 \le \omega \le 0.5$, $\Delta\xi < 0.2\%$ of ξ, $\Delta\eta < 0.005$ in each of the transformed regions, and $\xi_0 < 0.01$ the numerical solutions are independent of the grid structure. Note that, in the present study, the value of $\Delta\xi$ is varied relative to the local value of ξ to optimize the CPU time. With the use of a proper set of $\Delta\xi$, $\Delta\eta$, ξ_0, and ω, the relative error in the

computed results, that is, ξ_{max} and $\Delta_{1,max}$, is found to be less than 0.05%.

Results and Discussion

The velocity and temperature profiles for the baseline case at three different downstream locations, $\xi = 0.01$, 0.1, and 0.34, are shown in Fig. 4, where the locations $y/d = -1$ and 0 correspond to the center and the surface of the plate, respectively. At $\xi = 0.01$, the inner portion of the plate remains at its inlet temperature T_0 because the thermal wave has not yet penetrated through the plate. At this location, the plate can be treated as semi-infinite. At $\xi = 0.1$, on the other hand, the thermal wave has already penetrated through the entire thickness of the plate. The local temperature at the center of the plate is above its inlet temperature. It increases considerably in the downstream direction as ξ is increased from 0.1 to 0.34. The thermal boundary-layer thickness in the melt region also increases. Meanwhile, the local velocity has the constant value of U_0 from the center of the plate to the outer edge of the two-phase packing region, but beyond that point, it decreases to zero toward the edge of the momentum boundary layer in the melt region. Note that the momentum boundary layer is considerably thinner than the thermal boundary layer because the Prandtl number is small, that is, $Pr = 0.1$, for the baseline case.

The axial variations of the dimensionless thicknesses, Δ_1, Δ_p, and Δ_2 for the baseline case, are shown in Fig. 5. In Fig. 5, the finite

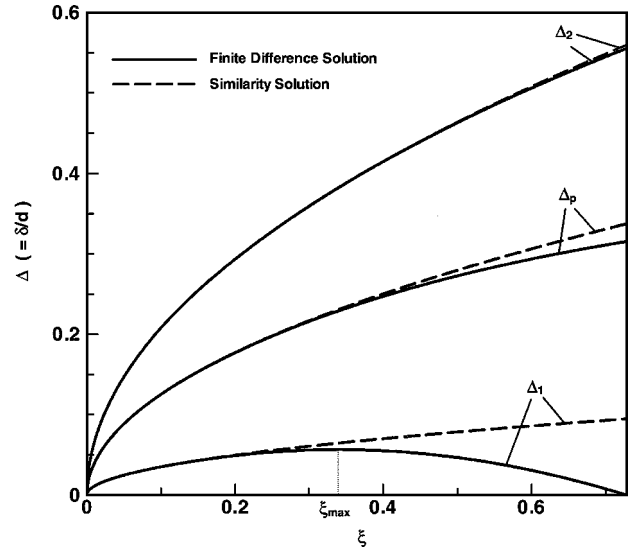

Fig. 5 Axial variation of the dimensionless freeze-coat thickness: comparison between the finite difference solution and the small-ξ similarity solution.

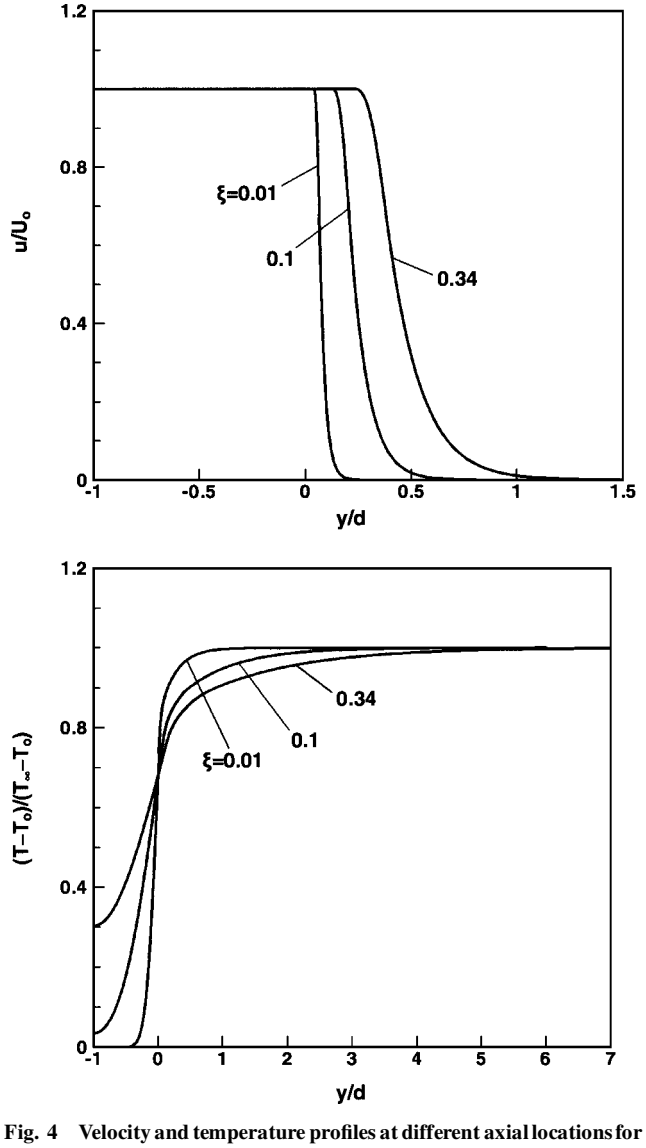

Fig. 4 Velocity and temperature profiles at different axial locations for the baseline case.

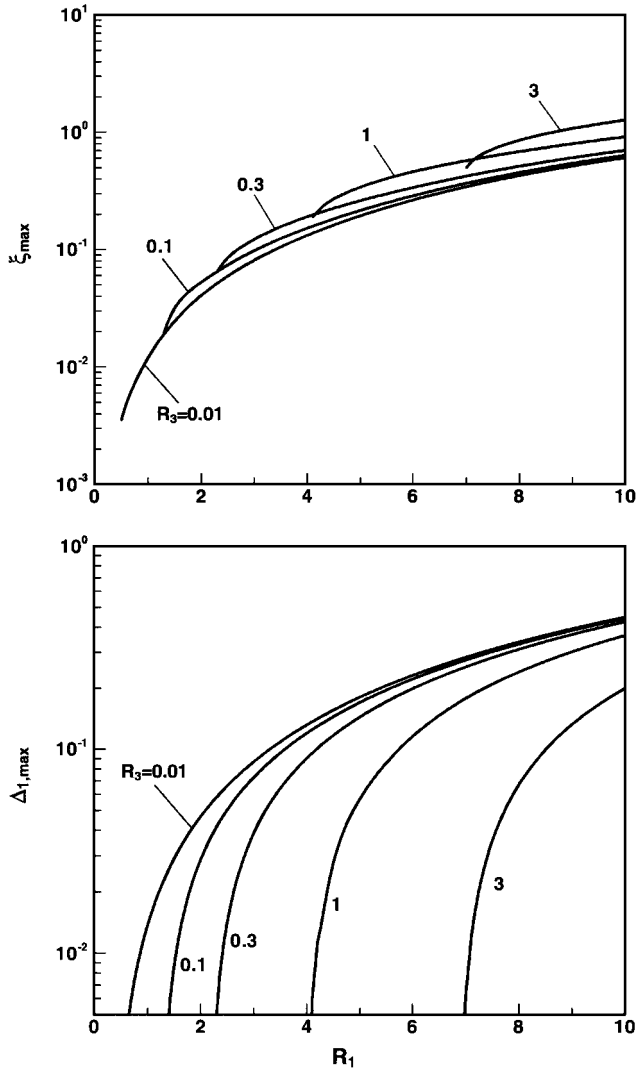

Fig. 6 Variations of the maximum freeze-coat thickness and the corresponding location with the wall subcooling parameter and the freeze coat-to-wall conductivity ratio.

difference solutions are compared with the similarity solutions for the limiting case of a semi-infinite wall,[13] for which the wall capacity is infinite, and as a result, Δ_1, Δ_p, and Δ_2 grow monotonically according to $\sqrt{\xi}$. On the other hand, for a finite plate, the freeze coat exhibits a growth and decay behavior because of a finite heat capacity of the plate. The freeze coat grows at first, reachs a maximum thickness at $\xi_{\max} = 0.34$, and then starts to decay, being completely remelted at $\xi = 0.72$. The maximum freeze-coat thickness is approximately 5% of the half-plate thickness. Note that, because of the growth of the thermal boundary layer, both Δ_p and Δ_2 continue to increase even though Δ_1 is decreasing in the decay regime where $\xi > 0.34$. From Fig. 5, it can be seen that, for $\xi < 0.15$, there is very little difference between the results obtained by the finite difference and the similarity methods. This further demonstrates that the use of the small-ξ solution as an initial condition for the finite difference scheme is valid.

Figure 6 shows the variations of $\Delta_{1,\max}$ and $\xi_{\max}$ with the wall subcooling parameter R_1 and the freeze coat-to-wall thermal conductivity ratio R_3. For a given R_3, both $\Delta_{1,\max}$ and $\xi_{\max}$ increase as R_1 is increased. It is obvious that the larger is the value of R_1, the more cooling is provided by the wall, leading to larger maximum freeze-coat thickness and the corresponding axial location. When R_1 is less than a certain value, no freeze coat is formed. For a given R_1, $\Delta_{1,\max}$ decreases with increasing R_3, whereas $\xi_{\max}$ increases with increasing R_3. Physically, under the same cooling condition, a wall material with a lower conductivity will conduct less heat through the wall. As a result, a thinner freeze coat is produced. Also, it will take a longer time for a freeze coat to reach the maximum thickness, leading to a larger value of $\xi_{\max}$. Note that, as R_3 approaches zero, an asymptotic behavior is obtained, corresponding to the case of maximum freeze-coat thickness that can be formed under a given set of cooling conditions.

Figure 7 shows the variations of $\Delta_{1,\max}$ and $\xi_{\max}$ with the wall subcooling parameter R_1 and the freeze coat-to-wall heat capacity ratio R_4. For a given R_4, $\Delta_{1,\max}$ and $\xi_{\max}$ increase with increasing R_1, similar to the behavior shown in Fig. 6. On the other hand, for a given R_1, $\Delta_{1,\max}$ and $\xi_{\max}$ increase with decreasing R_4. As R_4 is decreased, the heat capacity of the wall becomes larger, leading to larger value of $\Delta_{1,\max}$ and $\xi_{\max}$. A comparison of Figs. 6 and 7 indicates that $\Delta_{1,\max}$ and $\xi_{\max}$ is more sensitive to the change of R_4 than that of R_3. Thus, the heat capacity ratio R_4 plays a more significant role in the maximum thickness of the freeze coat under the same cooling conditions.

The effects of the wall subcooling parameter R_1 and the Stefan number *Ste* on $\Delta_{1,\max}$ and $\xi_{\max}$ are shown in Fig. 8. As expected, for a given Stephan number *Ste*, $\Delta_{1,\max}$, and $\xi_{\max}$ increase with increasing R_1. On the other hand, for a given R_1, $\Delta_{1,\max}$ and $\xi_{\max}$ increase as Stephan number is increased. A material with a smaller latent heat of fusion, that is, a larger Stefan number, will need to release less heat to the wall to form the same amount of freeze coat. Under the same cooling conditions, a thicker freeze coat will form as Stephan number is increased, leading to a larger value of $\Delta_{1,\max}$. Note that

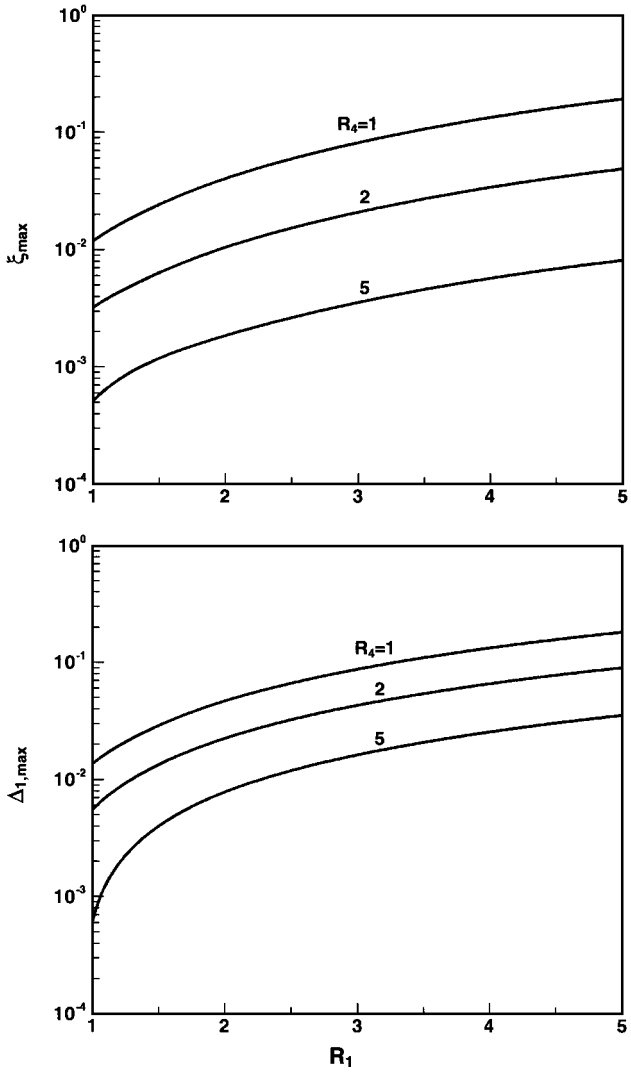

Fig. 7 Variations of the maximum freeze-coat thickness and the corresponding location with the wall subcooling parameter and the freeze coat-to-wall heat capacity ratio.

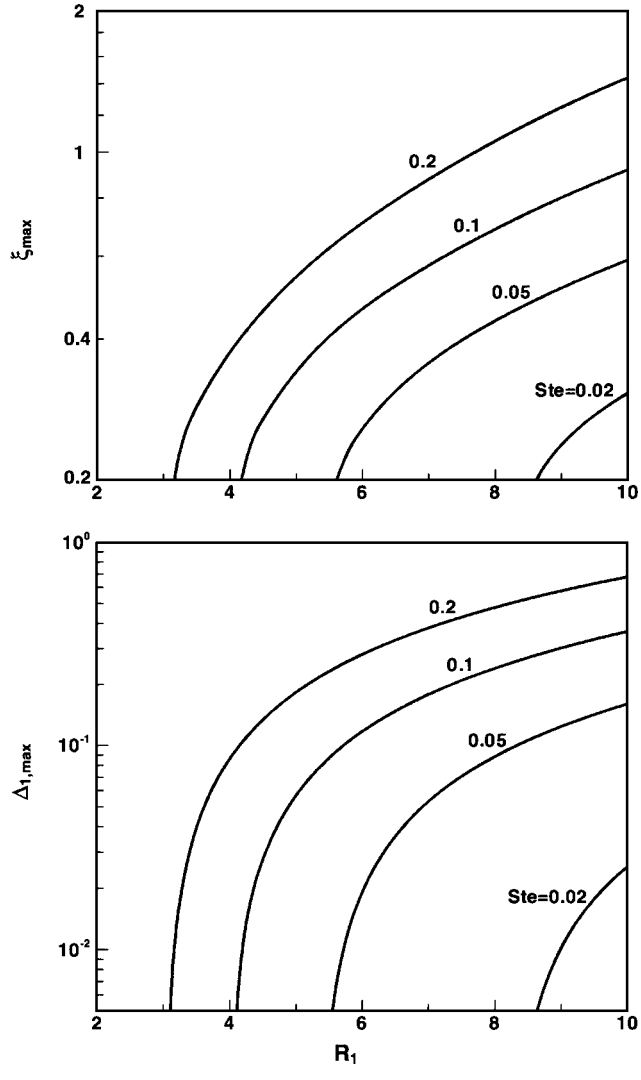

Fig. 8 Variations of the maximum freeze-coat thickness and the corresponding location with the wall subcooling parameter and the Stefan number.

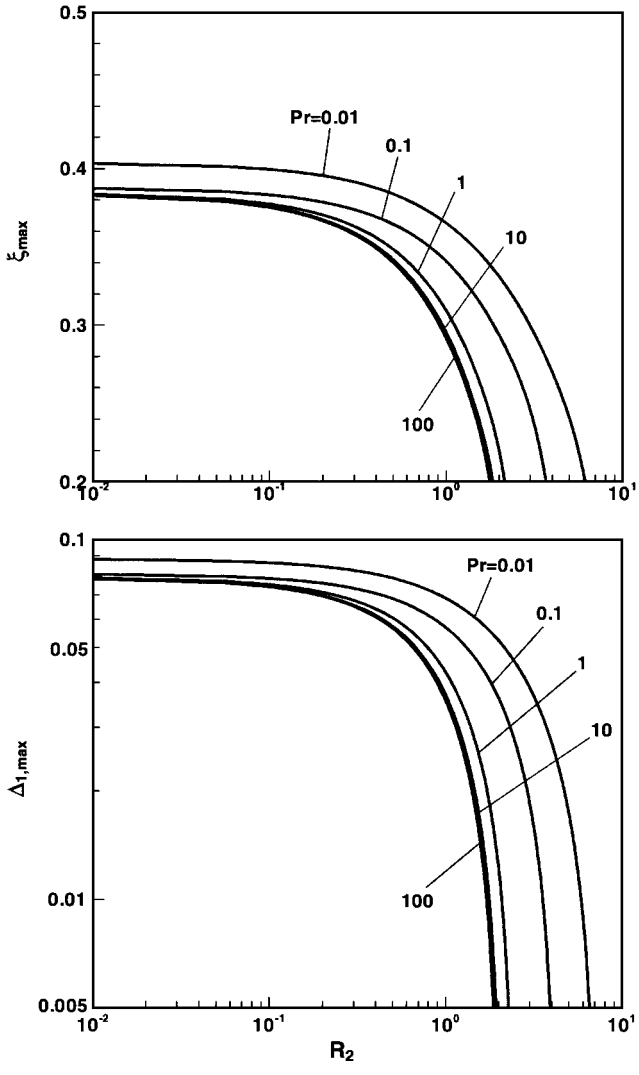

Fig. 9 Variations of the maximum freeze-coat thickness and the corresponding location with the melt superheating parameter and the Prandtl number.

ξ_{max} also becomes larger because it would take longer distance for the freeze coat to reach its maximum thickness.

Figure 9 shows the variations of $\Delta_{1,max}$ and ξ_{max} with the melt superheating parameter R_2 and the Prandtl number Pr. For a given Prandtl number Pr, both $\Delta_{1,max}$ and ξ_{max} decrease with increasing R_2. As the degree of liquid superheating is increased, more heat from the warm liquid will be convected to the freeze coat, leading to smaller values of $\Delta_{1,max}$ and ξ_{max}. Note that no freeze coat would form if R_2 exceeds a certain value. In contrast, for a saturated liquid, that is, R_2 approaches zero, $\Delta_{1,max}$ and ξ_{max} asymptotically approach their upper limits. For a given R_2, on the other hand, $\Delta_{1,max}$ and ξ_{max} increase with decreasing Prandlt number. This is expected because the convective heat transfer coefficient is smaller for a liquid with a smaller Prandlt number. The asymptotic behavior of a large-Prandlt-number liquid ($Pr > 10$) also can be seen in Fig. 9. Note that the effect of Prandlt number on $\Delta_{1,max}$ and ξ_{max} is considerably less than that of R_2.

Figure 10 shows the variations of $\Delta_{1,max}$ and ξ_{max} with the melt superheating parameter R_2 and the equilibrium partition ratio κ. For a given κ, $\Delta_{1,max}$ and ξ_{max} decrease with increasing R_2, similar to the behavior shown in Fig. 9. On the other hand, for a given R_2, $\Delta_{1,max}$ and ξ_{max} increase with increasing κ. As can be seen from Eq. (37), the amount of the solid fraction in the mushy region decreases as κ is increased. As a result, under the same cooling condition, more heat will be removed from the freeze coat to the plate, and a thicker layer of the freeze coat will be formed. When the results presented

Table 1 Variations of the maximum freeze-coat thickness and the corresponding location with the packing limit fraction for the baseline case

F_p	ξ_{max}	$\Delta_{1,max}$
0.50	0.3399	0.05645
0.55	0.3403	0.05664
0.60	0.3407	0.05683
0.65	0.3411	0.05701
0.70	0.3415	0.05720
0.75	0.3419	0.05740

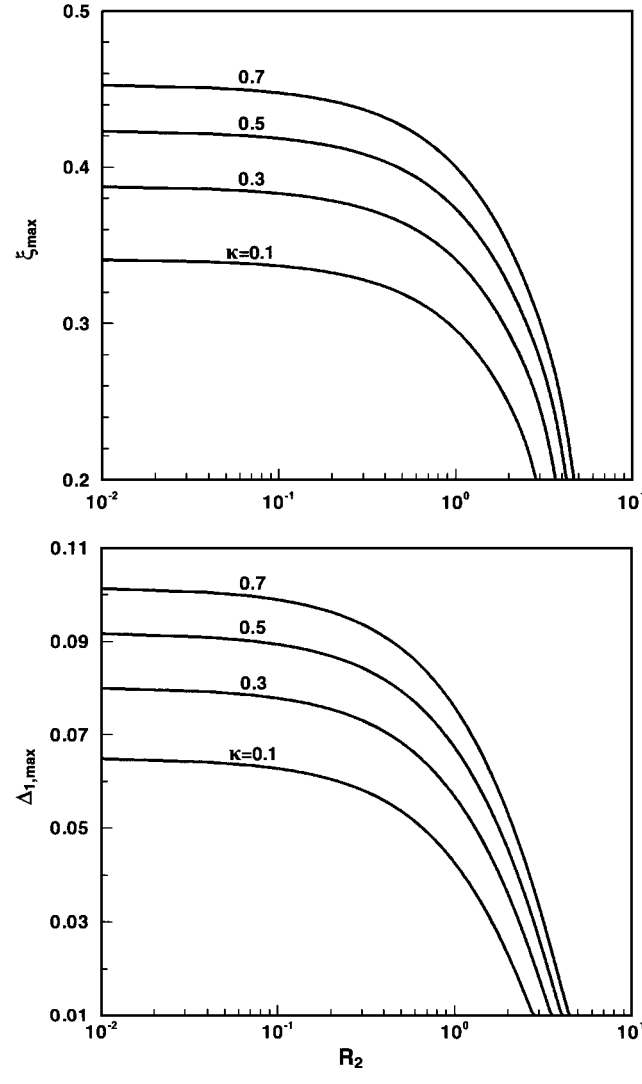

Fig. 10 Variations of the maximum freeze-coat thickness and the corresponding location with the melt superheating parameter and the equilibrium partition ratio.

in Figs. 9 and 10 are compared, it can be seen that $\Delta_{1,max}$ and ξ_{max} are more sensitive to the change of κ than that of Prandlt number.

The dependence of $\Delta_{1,max}$ and ξ_{max} on the packing limit F_p has been evaluated as shown in Table 1. It is found that, as the value of F_p is increased from 0.5 to 0.75, the values of $\Delta_{1,max}$ and ξ_{max} change only slightly. Hence, $\Delta_{1,max}$ and ξ_{max} can be considered insensitive to the variation of F_p. This result is consistent with that reported previously for the special case of an infinite wall thickness.[13]

The results on the growth and decay characteristics of a freeze coat should be useful for a designer to select the optimum operating conditions for the freeze-coating process. For given binary substance and wall material, appropriate immersion distance, inlet temperature, liquid bath temperature, and speed of the plate can be chosen to obtain the desired thickness of the freeze coat. Experimental data,

however, are needed to confirm the range of validity of the present model.

Conclusions

The process of freeze coating of a binary substance on a finite plate has been investigated numerically by a finite difference method. Based on the numerical results obtained in this study, the following conclusions can be made:

1) The growth and decay behavior of the freeze coat depends on eight dimensionless controlling parameters of the system. These are the wall subcooling parameter, the melt superheating parameter, the freeze coat-to-wall thermal conductivity ratio, the freeze coat-to-wall heat capacity ratio, the Prandtl number, the Stefan number, the equilibrium partition ratio, and the packing limit fraction.

2) The maximum freeze-coat thickness increases as either the wall subcooling parameter, the Stefan number, or the equilibrium partition ratio is increased. However, the maximum freeze-coat thickness decreases as either the melt superheating parameter, the freeze coat-to-wall thermal conductivity ratio, the freeze coat-to-wall heat capacity ratio, or the Prandtl number is increased. In the meantime, the corresponding axial location ξ_{max} increases as either the wall subcooling parameter, the freeze coat-to-wall thermal conductivity ratio, the Stefan number, or the equilibrium partition ratio is increased. On the other hand, ξ_{max} decreases as either the melt superheating parameter, the freeze coat-to-wall heat capacity ratio, or the Prandtl number is increased.

3) If the wall subcooling parameter is sufficiently low or the melt superheating parameter is sufficiently high, the freeze coat would not form due to insufficient cooling for latent heat removal from the melt to the moving plate.

4) An asymptotic behavior of the freeze coat is observed when either the melt superheating parameter approaches zero, that is, for a saturated liquid, the freeze coat-to-wall thermal conductivity ratio approaches zero, that is, for a highly conductive plate, or the melt Prandtl number becomes very large, that is, $Pr \geq 10$.

5) The maximum freeze-coat thickness and the corresponding axial location appear to be more sensitive to the change of the freeze coat-to-wall heat capacity ratio than that of the freeze coat-to-wall thermal conductivity ratio. Whereas the maximum freeze-coat thickness is very sensitive to the change of the melt superheating parameter and the Stefan number, the corresponding axial location is less sensitive to the variations of these two parameters. Both the maximum freeze-coat thickness and the corresponding axial location appear to be insensitive to the change of the packing limit fraction over the anticipated range of $0.5 \leq F_p \leq 0.75$.

References

[1]Kuiken, H. K., "Solidification of a Liquid on Moving Sheet," *International Journal of Heat and Mass Transfer*, Vol. 20, No. 4, 1977, pp. 309–314.

[2]Seeniraj, R. V., and Bose, T. K., "Freeze-Coating on a Continuous Moving Sheet and an Axially Moving Cylinder," *Wärme und Stoffübertragung/Thermo and Fluid Dynamics*, Vol. 15, No. 4, 1981, pp. 239–243.

[3]Cheung, F. B., "Analysis of Freeze Coating on a Non-Isothermal Moving Plate by a Perturbation Method," *Journal of Heat Transfer*, Vol. 107, No. 3, 1985, pp. 549–556.

[4]Cheung, F. B., "Thermal Boundary Layer on a Continuous Moving Plate with Freezing," *Journal of Thermophysics and Heat Transfer*, Vol. 1, No. 4, 1987, pp. 335–342.

[5]Rezaian, A., and Poulikakos, D., "Heat and Fluid Flow Processes During the Coating of a Moving Surface," *Journal of Thermophysics and Heat Transfer*, Vol. 5, No. 2, 1991, pp. 192–198.

[6]Stevens, R., and Poulikakos, D., "Freeze Coating of a Moving Substrate with a Binary Alloy," *Numerical Heat Transfer*, Pt. A., Vol. 20, No. 4, 1991, pp. 409–432.

[7]Zhang, H., Moallemi, M. K., and Kumar, S., "Thermal Analysis of the Dip-Coating Process," *Journal of Heat Transfer*, Vol. 115, No. 2, 1993, pp. 453–460.

[8]Zhang, H., and Moallemi, M. K., "Numerical Simulation of Hot-Dip Metallic Coating Process," *International Journal of Heat and Mass Transfer*, Vol. 38, No. 2, 1995, pp. 453–460.

[9]Cheung, F. B., and Cha, S. W., "Finite-Difference Analysis of Growth and Decay of a Freeze Coat on a Continuous Moving Cylinder," *Numerical Heat Transfer*, Vol. 12, No. 1, 1987, pp. 41–56.

[10]Cheung, F. B., Pellizzari, R. O., and Cha, S. W., "An Experimental Study of Freeze Coating on a Chilled Axially Moving Wire," *Experimental Thermal and Fluid Science*, Vol. 3, No. 4, 1990, pp. 431–439.

[11]Mahmoud, K. G., "Heat Transfer with Moving Boundary—Application to Transient Solidification of Warm Liquid on a Moving Cold Plate," *Computers and Chemical Engineering*, Vol. 17, No. 7, 1993, pp. 705–715.

[12]Mahmoud, K. G., "Numerical Analysis of Freeze Coating on a Two-Dimensional Moving Plate," *Numerical Heat Transfer*, Pt. A, Vol. 25, No. 3, 1994, pp. 279–293.

[13]Tangthieng, C., Cheung, F. B., and Shiah, S. W., "Behavior of the Two-Phase Mushy Zone During Freeze Coating on a Continuous Moving Plate," *Journal of Heat Transfer*, Vol. 124, No. 1, 2002, pp. 111–119.

[14]Krieger, I. M., "Rheology of Monodisperse Lactices," *Advances in Colloid and Interface Science*, Vol. 3, 1972, pp. 111–126.

[15]Ni, J., and Beckermann, C., "A Volume-Averaged Two-Phase Model for Transport Phenomena During Solidification," *Metallurgical Transactions B*, Vol. 22B, No. 3, 1991, pp. 339–361.

[16]Fukusako, S., Yamada, M., Horibe, A., and Kawai, A., "Solidification of Aqueous Binary Solution on a Vertical Cooled Plate with Main Flow," *Wärme und Stoffübertragung/Heat and Mass Transfer*, Vol. 30, No. 3, 1995, pp. 127–134.

[17]Cheung, F. B., and Epstein, M., "Solidification and Melting in Fluid Flow," *Advances in Transport Processes*, Vol. 3, 1984, pp. 35–117.

[18]Voller, V. R., Brent, A. D., and Prakash, C., "The Modelling of Heat, Mass and Solute Transport in Solidification Systems," *International Journal of Heat and Mass Transfer*, Vol. 32, No. 9, 1989, pp. 1719–1731.

[19]Yamada, M., Fukusako, S., Tago, M., and Horibe, A., "Freezing Characteristic along a Horizontal Cooled Tube Immersed in Aqueous Binary Solution with Main Flow," *Journal of Engineering Material and Technology*, Vol. 115, No. 1, 1993, pp. 54–62.

[20]Flemings, M. C., *Solidification Processing*, McGraw–Hill, New York, 1974, pp. 31–34.

[21]Einstein, A., "Eine neue Bestimmung der Molekuldimension," *Annalen der Physik*, Vol. 19, 1906, pp. 289–306.

[22]Krieger, I. M., and Daugherty, T. J., "A Mechanism of Non-Newtonian Flow in Suspensions of Rigid Spheres," *Transactions of the Society of Rhoelogy*, Vol. 3, 1959, pp. 137–152.

[23]Barnes, H. A., Hutton, J. F., and Walters, K., *An Introduction to Rheology*, Elsevier, Amsterdam, 1989, pp. 119–122.

[24]Crank, J., "How to Deal with Moving Boundaries in Thermal Problems," *Numerical Methods in Heat Transfer*, Wiley, New York, 1981, pp. 188–190.

[25]Cheung, F. B., Chawla, T. C., and Pedersen, D. R., "The Effects of Heat Generation and Wall Interaction on Freezing and Melting in a Finite Slab," *International Journal of Heat and Mass Transfer*, Vol. 27, No. 1, 1984, pp. 29–37.

[26]Anderson, D. A., Tannehill, J. C., and Pletcher, R. H., *Computational Fluid Mechanics and Heat Transfer*, McGraw–Hill, New York, 1994.